Maximizing the Dielectric Response of Molecular Thin Films *via* Quantum Chemical Design

Henry M. Heitzer, Tobin J. Marks,* and Mark A. Ratner*

Department of Chemistry and the Materials Research Center, Northwestern University, 2145 Sheridan Road, Evanston, Illinois 60208, United States

ABSTRACT Developing high-capacitance organic gate dielectrics is critical for advances in electronic circuitry based on unconventional semiconductors. While high-dielectric constant molecular substances are known, the mechanism of dielectric response and the fundamental chemical design principles are not well understood. Using a plane-wave density functional theory formalism, we show that it is possible to map the atomic-scale dielectric profiles of molecule-based materials while capturing important bulk characteristics. For molecular films, this approach reveals how basic materials properties such as surface coverage density, molecular tilt angle, and π-system planarity can dramatically influence dielectric response. Additionally, relatively modest molecular backbone and substituent variations can be employed to substantially enhance film dielectric response. For dense surface coverages and proper molecular alignment, conjugated hydrocarbon chains can achieve dielectric constants of >8.0, more than 3 times that of analogous saturated chains, ~2.5. However, this conjugation-related dielectric enhancement depends on proper molecular orientation and planarization, with enhancements up to 60% for proper molecular alignment with the applied field and an additional 30% for conformations such as coplanarity in extended π-systems. Conjugation length is not the only determinant of dielectric response, and appended polarizable high-Z substituents can increase molecular film response more than 2-fold, affording estimated capacitances of >9.0 μF/cm^2. However, in large π-systems, polar substituent effects are substantially attenuated.

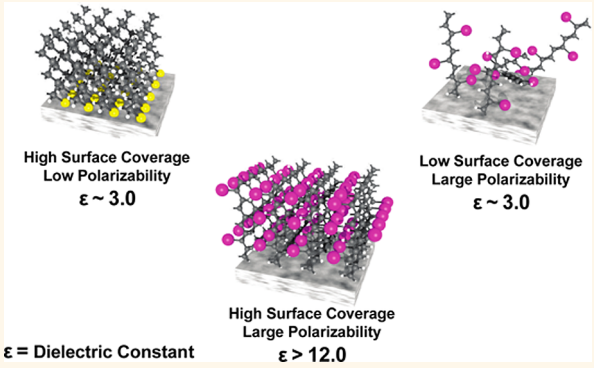

KEYWORDS: organic dielectric film · dielectric computation · field-effect transistor · self-assembled monolayer · density functional theory

Transistors are fundamental building blocks in all modern electronics, acting as on/off switches and signal amplifiers. Unconventional organic and inorganic field-effect transistors (FETs) have garnered significant interest because they offer unique properties such as light weight, mechanical flexibility, optical transparency, and suitability for low-cost roll-to-roll production *via* printing and related technologies.[1−4] These attractions make them ideal candidates for flexible, large-area applications such as information displays,[5−7] chemical sensors,[8−10] electronic paper,[2,11,12] and microelectronic logic circuitry.[13,14]

Due to lower production costs and potential fabrication by high-throughput printing or related techniques, OFET-based electronics remain an area of active interest.[15−17] However, a major obstacle in enhancing organic field-effect transistor (OFET) performance is the modest mobility of typical organic semiconductors and the low dielectric constants exhibited by typical organic gate dielectric materials. Regarding the latter materials, increasing the dielectric constant (high-*k* values) offers the opportunity of reducing OFET operating voltages and enhanced device efficiency. In the simplest embodiment, OFETs comprise three terminals, the source, drain, and gate, together with the organic semiconducting layer and an insulating (dielectric) layer. There are two different source-drain current operating regimes, described by[18] eqs 1 and 2, where W is the channel width, L the channel length, C the capacitance per unit area of the gate dielectric, and μ the field-effect mobility of the semiconductor. V_G and V_{SD} are the gate and source-to-drain voltages, and V_T is the

* Address correspondence to t-marks@northwestern.edu, ratner@northwestern.edu.

Received for review September 24, 2014 and accepted November 21, 2014.

Published online November 21, 2014
10.1021/nn505431p

threshold voltage (the gate voltage at which current begins to flow through the semiconductor).

$$(I_{SD})_{lin} = \frac{W}{L}\mu C\left(V_G - V_T - \frac{V_{SD}}{2}\right)V_{SD} \quad (1)$$

$$(I_{SD})_{sat} = \frac{W}{2L}\mu C(V_G - V_T)^2 \quad (2)$$

The linear regime occurs when $V_{SD} < V_G - V_T$, while $V_{SD} > V_G$ holds for the saturation regime. Increasing μ of the semiconductor or C of the gate dielectric will increase I_{SD}, enabling more efficient OFET function by decreasing the operating voltage. Equation 3 relates the capacitance, C, of a parallel-plate capacitor to the thickness d, the vacuum permittivity ε_0, and the dielectric constant ε. Traditionally, relatively thick[19] layers of SiO_2 have been used as OFET gate dielectrics. This thickness and relatively low dielectric constant of SiO_2 (ε = 3.9) results in unacceptable operating voltages.[16] While implementation of ultrathin SiO_2 dielectric layers increases the capacitance, it leads to unacceptable leakage currents[20] due to electron tunneling through the dielectric,[21,22] in addition to charge conduction observed in thicker films.[23,24]

$$C = \frac{\varepsilon_0\varepsilon}{d} \quad (3)$$

The functional minimum in SiO_2 dielectric thickness (~2−5 nm) requires the development of higher dielectric constant and low-leakage materials to enhance FET performance. Increasing dielectric constants in inorganic dielectrics typically correlate inversely with the band gap of the material,[25] also implying increased conductivity, hence increased FET current leakage between the source and the gate electrodes. Thus, any proposed strategy for new dielectric materials must accommodate a trade-off between dielectric performance and leakage current. Traditional organic materials generally exhibit small dielectric constants ($\varepsilon < 4.0$)[15,26,27] in comparison to conventional inorganic dielectrics such as HfO_2 ($\varepsilon \approx 17.0$).[16] Small capacitance in the gate dielectric layer requires undesirably high operating voltages to achieve useful current densities, and extensive research has been devoted to developing high-mobility organic and inorganic semiconductors for use in FET devices.[28−30] In contrast, the area of high-capacitance organic gate dielectrics has been far less extensively investigated.[15,16,31]

The rational design of high-dielectric constant organic materials has proven to be challenging. Most conventional dielectric measurements are made on highly disordered and/or polycrystalline solids, yet as will be seen here, molecular dielectric response can be highly anisotropic with respect to specific axes in molecular crystals, with certain axes exhibiting significantly larger dielectric constants than in the disordered bulk.[32,33] Note that ordered organic materials, arranged in monolayers, can exhibit relatively large dielectric responses,[34,35] with self-assembled monolayers (SAMs) enabling ultrathin, low-leakage dielectrics with capacitances of ~0.5 μF/cm^2,[36] affording OFET operating voltages in the promising <5 V regime.[15,31] In addition to SAMs, recent work has reported promising results with organic polymers.[37] Nevertheless, higher dielectric constants would be desirable, and to date, there has been no systematic effort to design high-dielectric response organic materials that has focused on understanding the polarizability of the constituent molecules, that is, a molecular design approach. There has been no systematic study of how materials properties, such as molecular architecture, surface coverage, and surface binding geometry, govern molecular and, ultimately, thin-film dielectric response. Indeed, it will be seen here that molecular level materials properties can significantly enhance thin-film dielectric performance, and conversely, an otherwise ideal material may exhibit poor dielectric response due to suboptimal molecular arrangement within an FET. While we primarily focus on how dielectric performance can be tailored for FET devices, altering the local dielectric behavior of a molecular system should be useful in manipulating other important chemical phenomena as diverse as organic photovoltaic,[38,39] electron transfer,[40,41] and chemical sensing functions.[8,9,42]

The focus of this contribution is to systematically elucidate the effects of molecular and multimolecular chemical properties on thin-film dielectric response using a first-principles theoretical technique that can accurately describe the macroscopic dielectric response of molecule-based materials. Conventional modeling approaches have utilized the Clausius−Mossotti[43] relationship to obtain the macroscopic dielectric constants by relating them to the microscopic polarizabilities (α) of the constituent molecules.[44] While effective in many cases, the Clausius−Mossotti relation is not generally valid for modeling multimolecular condensed-state organic systems due to the limitations of conventional quantum chemical approaches which simplistically assume isolated molecules in vacuum, ignoring crucial bulk properties inherent to the macroscopic dielectric response and thus overestimating polarizability.[45] A more natural way to model the electronic properties of ordered bulk systems involves the implementation of periodic boundary conditions in conjunction with density functional theory (DFT).[33,46,47]

In this contribution, we focus on the dielectric behavior of molecular hydrocarbons arranged in monolayers. Monolayers are chosen because their structures approximate thin films and allow an examination of the bulk properties of a multimolecular material while providing insight into the dielectric response of individual molecules.[33] Experimentally, monolayers have been grown with both simple alkyl

chains and highly conjugated π-blocks; the objective here is to understand which systems produce the largest dielectric response and to correlate important chemical characteristics of SAM molecular architecture, surface coverage, and surface binding geometry, with dielectric response. This level of analysis is important since molecules can have multiple, nearly iso-energetic geometrical configurations that can substantially modulate electronic properties such as dipole moment,[48] band gap,[49] and charge transport.[50] Additionally, tension and strain can induce changes in molecular and multimolecular geometries[51] and are known to alter the bulk dielectric properties of organic materials[52] in ways we investigate here. Finally, we sequentially examine various conjugated backbones and simple molecular substitutions to determine the effects of these molecular modifications on monolayer dielectric response. By analyzing selected model systems, insight is provided into the dielectric response in organic materials and new materials design rules emerge for high-capacitance organic gate dielectrics.

RESULTS

In the following sections, we first examine the local dielectric response of sparsely covered molecular monolayers consisting of alkane and alkyne chains. The component molecular structures, surface coverage and tilt angle, and π-system planarity in donor−acceptor-substituted biphenyls are systematically altered to determine how they affect dielectric film dielectric properties. Chemical alterations such as molecular substitution on alkyne chains, π-conjugated backbones, and phthalocyanine molecules are used to tailor dielectric response in molecular monolayer materials. Finally, a comparison of the present computed results with experimental values and analysis of functional choice is shown to demonstrate the validity of our results.

We implement two finite difference techniques, referred to as the local dielectric method[33] and the dipole method,[45] to calculate the dielectric response of a monolayer. The methods are identical in implementation except for the processing of data. Both methods have shown to be very accurate over a host of inorganic and organic materials.[33,45,53−56] For clarity, any dielectric values reported using the local dielectric method will be reported using $\eta(z)$, the local dielectric constant, while dielectric results obtained using the dipole method will be reported as ε, the average dielectric constant of the monolayer. A typical simulation cell is shown in Figure 1. A single molecule is placed inside a unit cell and is infinitely repeated in the *x* and *y* directions using periodic boundary conditions that simulate a monolayer. In the *z* direction, a 15 Å vacuum layer is inserted to simulate a monolayer—this ensures no interaction between layers. The system is first relaxed in the absence of an electric field, in the corresponding molecular packing arrangement of interest. After the system is relaxed, two electric fields are applied parallel to the *z* axis. Differences in charge density and dipole moment enable the determination of the dielectric constant as detailed in the Methods section.

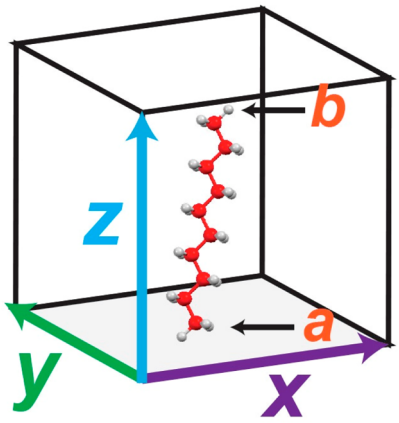

Figure 1. Schematic portrayal of a representative unit cell for dielectric response computation. A single molecule repeated infinitely in the *x* and *y* directions representing a single monolayer. The applied electric field parallel to the *z* axis and the thickness of the monolayer are determined by the *z* position of points *a* and *b*.

Local Dielectric Response in Hydrocarbon Monolayers. SAMs have recently been used in a variety of dielectric systems, including those for OFETs, and have achieved $C > 0.5\ \mu F/cm^2$.[36,57] Components ranging from simple thiolated alkane chains to elaborate, highly conjugated π-systems have been used to fabricate such monolayers. Based on chemical intuition, conjugated species would seem likely to offer larger dielectric responses due to their larger polarizabilities. To verify and quantify this conjecture, two sparsely covered (1 molecule/nm^2) monolayers are first modeled, one consisting of a 10 carbon saturated alkane chain (hereafter referred to as a polyethylene) and the other consisting of a 10 carbon chain of alternating single and triple bonds (hereafter referred to as a polyyne). Note that a sparse monolayer is used initially to ensure minimal interaction between the molecules. This sparse coverage leads to relatively low dielectric constants and is not intended to represent a physically realistic system. The molecules here are oriented parallel to the applied electric field.

In Figure 2, the local optical and static dielectric profiles are shown for polyethylene and polyyne. The local optical and static dielectric constants are nearly identical in each system. This is expected since the major difference between the static and optical dielectric response in solid-state systems is due to the polar bonds that comprise the molecular structures.[33] Thus, in pure hydrocarbon systems, where there is little polar bonding, negligible differences in the local optical and static dielectric profiles are observed. For pure hydrocarbon systems, only the optical dielectric response ($\eta(z) = \eta_{opt}(z)$) is reported here due to the close overlap

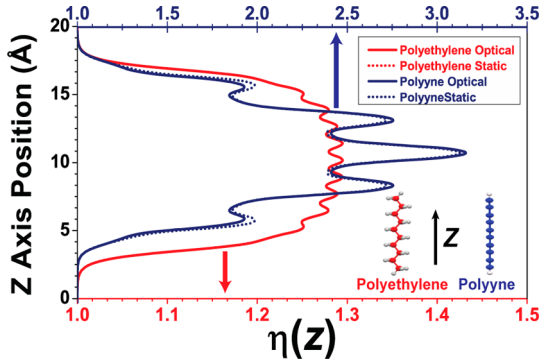

Figure 2. First-principles DFT computation of the local optical and static dielectric responses for polyethylene and polyyne monolayers. There is an enforced 10 Å separation in the *x* and *y* directions between all molecules, and the polarization is planar averaged over *x* and *y*. Computed local optical (solid) and static (dashed) dielectric constants of polyethylene (red) and polyyne (blue) SAMs. The bottom (red) *x* axis corresponds to the polyethylene response, while the top (blue) *x* axis corresponds to the polyyne response. The local and static dielectric profiles of polyethylene are indistinguishable, making it appear that only one is plotted. The applied electric fields parallel to the *z* axis have a strength of ±0.001 au. A *k*-point scheme of 2 × 2 × 2 is used for all simulations, and the polymers are represented by 10 carbon chains (as shown).

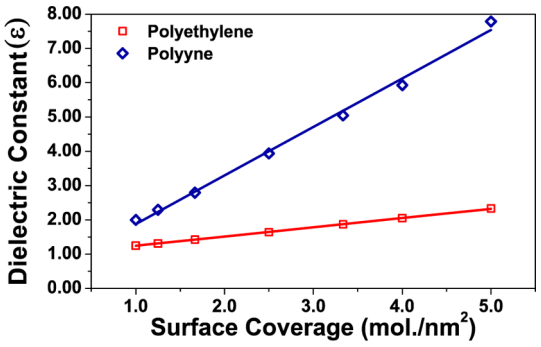

Figure 3. First-principles DFT calculation of the optical dielectric constant for polyethylene and polyyne monolayers as a function of surface coverage in molecules/nm^2. Calculated optical dielectric constant for polyethylene (red squares) and polyyne (blue diamonds) 10 carbon oligomers as a function of surface coverage. Solid lines are fitted with a linear regression. For each surface coverage, molecules are separated such that the *x* and *y* distances between neighboring molecules are identical. The molecules are also assumed to be standing perpendicular to the surface (parallel to the applied electric field). The applied electric fields are parallel to the *z* axis and have a strength of ±0.001 au. A *k*-point scheme of 2 × 2 × 2 is used for all simulations.

between the optical and static dielectric profiles. In systems containing elements besides C and H, both optical and static dielectric constants are reported. It is also clear that the conjugated polyyne has a significantly larger dielectric response than the saturated polyethylene. From eq 9, the calculated observable dielectric constants are computed to be $\varepsilon = 1.22$ and $\varepsilon = 1.94$ for polyethylene and polyyne, respectively. This is because the electrons in the π-system are more responsive to the electric field, inducing a more polarized environment and therefore a larger dielectric response. Note also that in polyethylene the dielectric response quickly reaches a maximum that spans the length of the molecule, while the polyyne response builds over the length of the molecule, reaching a maximum at the center. This indicates that the electrons have greater susceptibility to polarization at the center of the π-system.[5−7,45] High local dielectric constants in conjugated π-systems have important implications for OPVs where the low dielectric constant of organic materials is often cited as the principal reason for the high exciton binding energies *versus* those in traditional inorganic photovoltaic materials.[8−10,58] Thus, installing high local dielectric environments in conjugated materials is a potential avenue for reducing OPV exciton binding energies.

Surface Coverage Effects on Dielectric Response. SAMs exhibit variable surface coverage densities depending on the nature/energetics of the substrate−molecule and molecule−molecule interactions as well as the details of the film deposition technique.[2,11,12,59,60] Determining the relationship between the surface coverage of a particular molecule and the resulting dielectric response should be useful in designing new OFET gate dielectric materials. To examine the role of surface coverage in SAM dielectric response, the surface coverage was varied from sparsely (0.1 adsorbed chain per nm^2) to densely (5.0 adsorbed chains per nm^2) packed in a square lattice—equal spacing in the *x* and *y* directions between molecules. Dense is defined as the maximum reported surface coverage of linear alkanethiol chains that can be achieved experimentally on single-crystal Au surfaces.[13,14,46,47,61] The polyethylene and polyyne-based SAMs were chosen to assess possible trend differences between nonconjugated and conjugated materials as the surface coverage/packing is increased. Molecular long axes are assumed to be oriented parallel to the electric field, and tilt angle effects are addressed in the following section. Since PBE and other functionals can overestimate polarization in extended conjugated systems, our calculations most likely represent upper bounds on the dielectric constant but nevertheless reveal instructive trends.[15−17,62−66] An examination of functional choice is given in the model validation section that follows.

Figure 3 shows the relationship of the computed dielectric constant to the surface coverage for the two different (polyethylene and polyyne) hydrocarbon SAM systems. In both systems, the dielectric constant increases linearly with the surface coverage, in agreement with other studies.[18,45,67] This behavior can be explained by the incremental replacement of the vacuum, $\varepsilon = 1$, with hydrocarbon chains as the surface coverage increases. By removing the vacuum and replacing it with an electron-rich (*versus* vacuum) molecular material, the density of electrons that can respond to the applied field is increased, thereby increasing the dielectric response. This behavior is

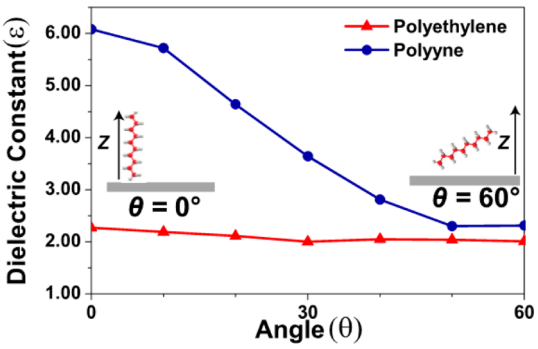

Figure 4. First-principles DFT calculation of the optical dielectric constant of C-10 polyethylene and polyyne monolayers as a function of molecular tilt angle from the surface normal. Computed dielectric constants are shown for polyethylene (red triangles) and polyyne (blue circles) as a function of the tilt angle in degrees. For reference, at 0°, the molecular long axis is oriented parallel to the applied electric field. The molecules are separated by 5 Å in the *x* and *y* directions. The applied electric fields are parallel to the *z* axis and have a strength of ±0.001 au. A *k*-point scheme of 2 × 2 × 2 was used for all simulations.

similar to increasing the surface dipole moment as a function of surface coverage.[68,69] Remarkably, at high surface coverage, the simple polyyne hydrocarbon has a computed dielectric constant >8.0. At ε = 8.0, the corresponding capacitance of a polyyne monolayer having a 1.3 nm estimated thickness, calculated using eq 3, is $C \sim 5.0\ \mu F/cm^2$— a value significantly greater than any of the "champion" gate dielectrics prepared and characterized to date.[19,34,70,71] These results point to an important design guideline for creating high-capacitance molecular gate dielectrics: all other factors being equal, maximizing the surface coverage of an oriented molecular material should achieve the maximum dielectric response. Dense surface coverage allows SAMs composed of relatively simple molecules, such as a polyyne, to achieve noteworthy dielectric response.

Molecular Orientation Effects on Dielectric Response. The orientation of SAM molecules on a surface can vary greatly depending on their particular structures.[16,60] To investigate the effects of molecular orientation on thin-film dielectric response, the alignment angles of the polyethylene and polyyne long axes were varied from 0 to 60° with respect to the surface normal. Hereafter, 0° refers to molecular alignment perpendicular to the substrate plane (*i.e.*, parallel to the electric field direction). Beyond 60°, the hydrocarbon molecules come into contact with one another, as seen by examining the periodic system with van der Waals radii, at a surface coverage of 4 molecules/nm^2, the density used in this simulation. Figure 4 depicts the dielectric constant of C-10 polyethylene and polyyne SAMs as a function of tilt angle. While the dielectric constant of the polyethylene SAM remains essentially unaffected as the angle is increased ($\Delta\varepsilon < 0.2$), there is a large variation of the polyyne SAM dielectric constant as θ is increased from 0 to 60°. In this simulation, there is over a 60% reduction in the dielectric response of the polyyne, and the axis is tilted from 0 to 60°. Decreasing the dielectric constant by 60% leads to a substantial fall in capacitance, which is expected to diminish TFT performance (eqs 1 and 2). The dependence of the dielectric response on orientation angle in polyyne SAMs reflects changes in the interaction of the π-system with the electric field. When the molecular long axis is parallel to the electric field, the π-electrons can respond over the entirety of the π-pathway. As the molecule is brought normal to the electric field, there is less efficient coupling along the molecular length, leading to a decreased dielectric response. This phenomenon is not observed in the polyethylene SAM since there is no π-system. Clearly, to achieve large dielectric responses, conjugated π-electron SAMs must be properly oriented in the electric field direction.

Molecular Architecture Effects on Dielectric Response. Many molecules are conformationally dynamic, sampling a variety of molecular geometries, with structural interconversion rates sensitive to factors such as temperature, solvation, packing, and surface binding.[20,72−74] With such geometrical fluctuations, experimental capacitance measurements on bulk molecular systems are necessarily an ensemble assay, sampling numerous geometric configurations. Indeed, it has been shown that small changes in geometry can have a significant effect on bulk electronic properties.[21,22,48−50] It is thus of interest to inquire how various geometric configurations affect molecular dielectric response. Note however that it is nontrivial to incorporate such geometric fluctuations into DFT calculations due to the computational complexity of sampling so many different configurations. Thus, this analysis will be restricted to simpler systems.

Biphenyls are known to have multiple energetically accessible rotamers about the aryl−aryl bond, dependent on the chemical environment and the various substituents appended to the biaryl skeleton.[23,24,75,76] The biaryl π-system is an ideal bridge for "push−pull" behavior as seen in donor−bridge−acceptor (D−bridge−A) structures,[15,26,27,77] and for this reason, donor and acceptor groups are introduced here at the 4,4′ positions of the biphenyl skeleton. In this particular example, the donor group is NH_2 and the acceptor group is NO_2. For simplicity, this donor−biphenyl−acceptor molecule is referred to as DBiphA. With the introduction of polar bonds, the static dielectric constant is expected to differ significantly from the optical dielectric constant, so both values are reported here. Figure 5A shows DBiphA at various dihedral angles, Φ, from coplanar, and Figure 5B depicts the static and optical dielectric constants of DBiphA SAMs as a function of intramolecular Φ. At Φ = 0°, the two phenyl rings (and π-systems) are coplanar, while at Φ = 90°, they are orthogonal. Note that both static and optical dielectric constants at Φ = 0°

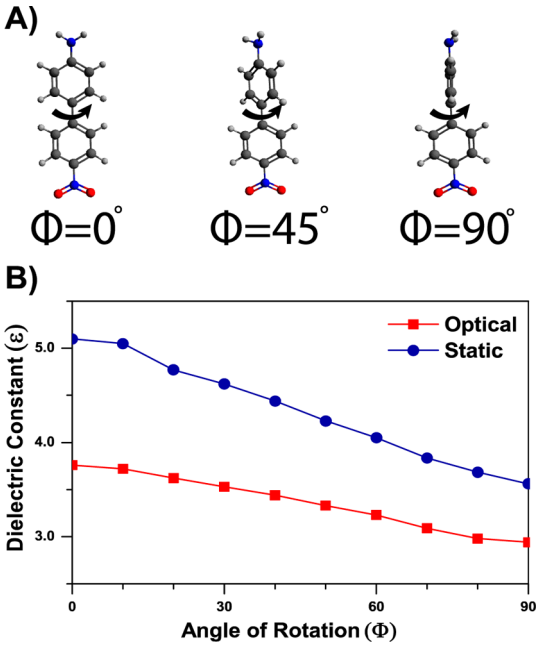

Figure 5. First-principles DFT calculation of the optical and static dielectric constants of *p*-H_2N-biphenyl-NO_2 (DBiphA) SAMs as a function of aryl−aryl bond dihedral angle. (A) DBiA at 0, 45, and 90° dihedral angles (Φ) about the arene−arene bond. (B) Static (blue squares) and optical (red circle) dielectric constant at different Φ values from 0 to 90°. The biphenyl unit cell contains one molecule and has dimensions of 6.25 × 6.25 × 25.0 Å. The molecular long axes and applied electric fields are parallel to the *z* axis with a field strength of ±0.005 au. A *k*-point sampling scheme of 2 × 2 × 2 is used for each material.

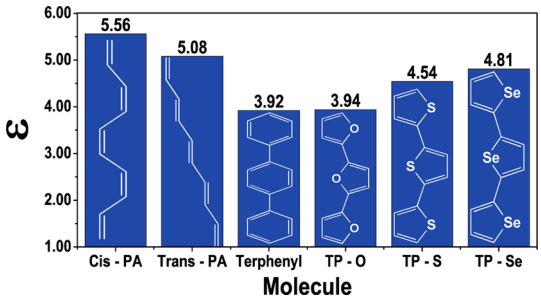

Figure 6. First-principles DFT calculation of the static dielectric constants of SAMs having varied modes of conjugation. Structures of the various molecules studied are shown in white on the bar graph, with static dielectric constant of the various SAMs displayed above. The unit cell contains one molecule and has dimensions of 5.47 × 5.47 × 25.0 Å. The applied electric fields are parallel to the *z* axis and have a strength of ±0.001 au. A *k*-point sampling scheme of 2 × 2 × 2 is used for each material.

($\varepsilon_{opt.}$ = 3.76, ε_{static} = 5.09) are significantly larger than at Φ = 90° ($\varepsilon_{opt.}$ = 2.94, ε_{static} = 3.51). At Φ = 90°, the π-delocalization is discontinuous at the linking bond, weakening the donor−acceptor interaction. It is reasonable that this π-electron confinement leads to diminished dielectric response by suppressing electron cloud polarization by the electric field. This confinement is similar to other localization effects observed in conjugated molecules when distortions of this type disrupt molecular planarity.[16,78]

These results demonstrate the importance of molecular architectural parameters in modulating dielectric response. As shown in Figure 5B, the average dielectric constant of the DBiphA SAMs drops substantially as Φ approaches 90°. This dihedral angle can, of course, be manipulated *via* substituents, especially by introducing multiple *ortho* substituents on the phenyl rings,[28−30,79] thereby tuning the film bulk dielectric response. It is evident then that the successful design of molecule-based high-capacitance dielectric materials should capitalize on the power of adjusting molecular conformational architecture to achieve desired dielectric response.

Tailoring the Molecular Backbone for Dielectric Response. As shown above, molecular properties such as surface coverage density, molecular tilt angle, and molecular conformation can have large effects on the bulk dielectric response of a given molecular film. While such properties are important, we now examine π-architecture in greater detail. Several different conjugated backbones are shown in Figure 6, with *cis*-PA and *trans*-PA being C-10 polyacetylene isomers. TP−X are different forms of trimeric four-carbon O, S, and Se heterocycles. Computed static dielectric constants for these molecular monolayers are shown in Figure 7 at equivalent surface coverages (3.33 molecules/nm^2). Note that the film dielectric constants vary over a moderate range of ∼4.0−5.5. Specifically, terphenyl exhibits the smallest response at 3.92, which can be partially explained by intramolecular twisting (∼20° energy-minimized dihedral angle, similar to experimental dihedral angles in biphenyl)[15,16,31,75,76] about the aryl−aryl bonds, disrupting the structural coplanarity and reducing the π-cloud polarization. The other molecular films examined exhibit far less interruption of the planarity. The difference in dielectric response between *cis*-PA and *trans*-PA is due to the compressed length of the former molecule, ∼1.5 Å *versus trans*-PA. This difference in conjugation length induces a moderate change in dielectric response even though both molecules exhibit similar changes in dipole moment and have the same number of π-electrons. The TP−X series illustrates the trend that introduction of larger/higher *Z* heteroatoms leads to increased dielectric response, Se > S > O. Thus, altering the conjugated backbone has modest effects on the dielectric response; however, as illustrated by terphenyl, it is important that the molecular backbone is locked into a planar confirmation to ensure maximum dielectric response.

Effects of Polar Substituents on Dielectric Response. In the foregoing discussion, the effects of altering the conjugated backbones of SAM molecular constituents on bulk dielectric properties is examined. The next logical step is to inquire how different backbone substituents alter the dielectric response. In Figure 7A (left) is shown the model conjugated backbone, *trans*-PA, with a single substituent group R introduced.

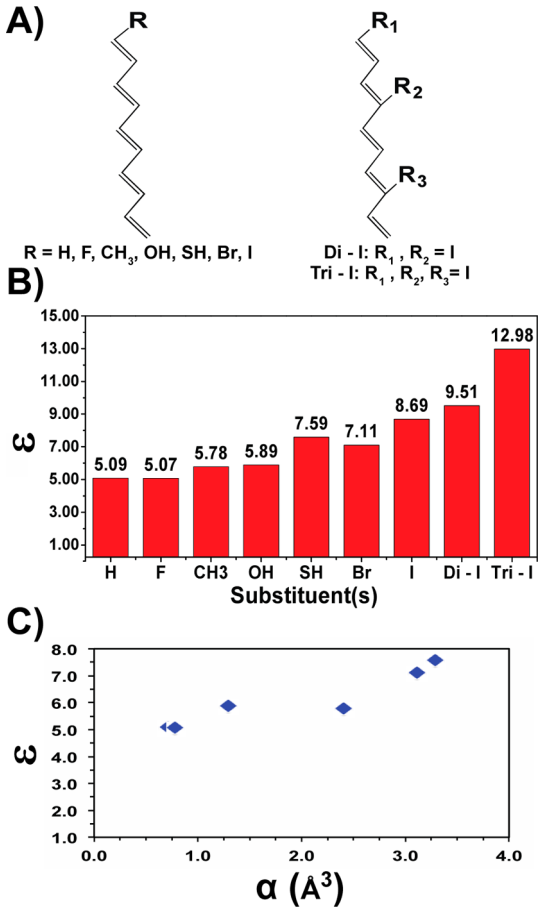

Figure 7. First-principles DFT calculation of the static dielectric constants of SAMs having various molecular backbone substituent(s). (A) Left: a monosubstituted *trans*-polyacetylene with replacement of a terminal H atom. Right: di- and trisubstituted polyacetylenes with the second and third substitutions taking place at the backbone positions indicated. (B) Static dielectric constant of the various monolayers. The unit cell contains one molecule and has dimensions of 5.47 × 5.47 × 25.0 Å. The applied electric fields are parallel to the *z* axis and have a strength of ±0.001 au. A *k*-point sampling scheme of 2 × 2 × 2 is used for each material. (C) Calculated dielectric constant of substituted *trans*-polyacetylenes (ε) *versus* polarizability of the substituent (α). Polarizability of substituents is calculated using finite differences with the ωB97X functional and a aug-cc-PVDZ basis set.

In principle, replacing H with other substituents might increase the dielectric response since H is a small, relatively nonpolarizable atom. In place of H, substituents of varying sizes and polarizabilities (F, CH_3, OH, SH, Br, and I) are next introduced, and the computed static dielectric responses at equivalent surface coverages (3.33 molecules/nm^2) are shown in Figure 7B. Note that the dielectric response increases in all cases except when H is replaced with F, which has similar polarizability. In contrast, incorporation of SH, Br, and I significantly increases the dielectric response in accord with their increased polarizabilities. To quantify this result, in Figure 7C substituent polarizabilities (α) are plotted *versus* calculated dielectric constant (ε) of the substituted polyacetylenes. Since polarizabilities

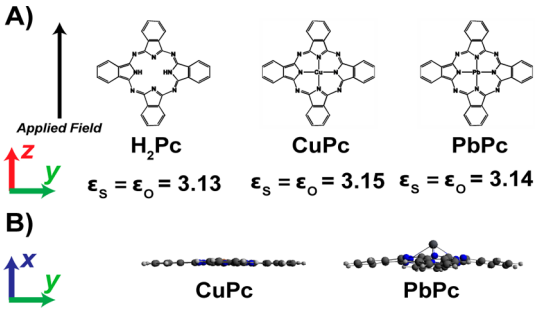

Figure 8. First-principles DFT calculation of the optical and dielectric constants of phthalocyanine SAMs having various substituents. (A) Structures of three different phthalocyanine complexes, unsubstituted phthalocyanine (H_2Pc), copper phthalocyanine (CuPc), and lead phthalocyanine (PbPc). Optical and static dielectric constants are reported below each compound. The unit cell contains one molecule and has dimensions of 4.0 × 16.0 × 30.0 Å. The applied electric fields are parallel to the *z* axis and have a strength of ±0.001 au. A *k*-point sampling scheme of 2 × 2 × 2 is used for each material. (B) View of CuPc and PbPc along the *z* axis, showing CuPc is planar while PbPc has buckled geometry. H_2Pc has a structure similar to CuPc.

are not generally known for open shell/radical substituents, the polarizabilities of the hydrogenated species (HF, CH_4, H_2O, H_2S, and HBr) are used. Note that HI does not have an aug-cc-PVDZ basis set implemented in GAMESS and is therefore omitted from this comparison. Note the significant positive correlation (R^2 = 0.863) between substituent polarizability and the substituted polyacetylene calculated dielectric response.

Remarkably, even the introduction of a single substituent atom can substantially increase the calculated *trans*-polyacetylene dielectric constant from ~5.0 to ~8.5 in dense molecular films. To investigate further how substitution modulates dielectric response, additional H atoms are next replaced with iodine atoms as shown in Figure 7A (right), and the resulting static dielectric constants are plotted in Figure 7B. Note that 2-I and 3-I exhibit progressively larger dielectric constants, with 3-I achieving a remarkable computed dielectric constant of 12.98. This corresponds to a thin-film capacitance exceeding 9.0 μF/cm^2. As shown above, at high surface coverages and with proper molecular alignment, even simple molecular structural changes can dramatically increase the dielectric response of a thin molecular film and high-capacitance organic thin-film dielectrics are clearly possible.

2-D Conjugation. Phthalocyanines. The above discussion illustrates how dielectric responses can be modulated by changing molecular conjugation schemes and introducing polarizable substituents. We next explore the interplay between conjugation and skeletal substitution using metal-free phthalocyanine (H_2Pc) and two metal complexes, copper phthalocyanine (CuPc) and lead phthalocyanine (PbPc), shown in Figure 8A. H_2Pc has a plausibly polarizable, many-electron π-system and might be expected to exhibit a large

dielectric response, perhaps further enhanced by incorporation of metal ions in the central molecular core. Interestingly, however, the computation shows that there is negligible difference between the optical and static dielectric constants, indicating that the dielectric response is derived from electronic responses, presumably from the π-system. H_2Pc has the smallest dielectric response, but only slightly below that of CuPc and PbPc, indicating that ostensibly polarizable substituents have little importance in the dielectric response of these highly conjugated molecules. These results comport well with other computational studies showing that the polarizability of Pc molecules is invariant to substituents with the field applied both parallel and perpendicular to the molecular plane.[32,33,80] An interesting point to note here is that the computed PbPc dielectric constant is less than that of CuPc even though the Pb atom is far more electron-rich than Cu. Examining optimized geometries of each molecule shows that PbPc is nonplanar with a cup shape (confirmed experimentally),[34,35,81,82] while CuPc has a planar π-system (Figure 8B). The nonplanarity slightly diminishes the π-conjugation in PbPc, inducing a minor decrease in dielectric response *versus* CuPc, while intuitively an increase might be expected.

Model Validation. Calculations using the present technique are highly efficient, primarily depending on unit cell size. Comparison to experiment is unfortunately difficult as there is a dearth of reported dielectric data for molecular monolayers. Dielectric constants in the range $\varepsilon_{exp.} = 2.00-3.00$ have been reported[27,36,83−85] for 10 carbon chain alkanelthiol SAMs at a surface density of ~4.5 mol/nm^2, which is in good agreement with the present calculation, $\varepsilon_{theory} = 2.66$, and experimental dielectric constants for similar alkyl SAMs.[15,16,31,84−87] We were unable to find experimental dielectric constant values for other molecular monolayer materials outside a class of complex chromophores designed by this group.[15,35,38,39,57,88] This technique has been applied to a host of different materials such as CuPc,[40,41,80,89] polar and nonpolar molecular crystals,[8,9,33,42] and a host of different oxide materials,[43,53−56,90] with very good agreement with experiment.

The PBE functional is chosen for its widespread use in plane-wave DFT. More complex, computationally intensive functionals are available; however, it is not obvious that their accuracy is better. To benchmark PBE performance against other functionals, identical simulations were performed using the Coulomb potential screening hybrid functional by Heyd, Scuseria, and Ernzerhof (HSE) 06 and a GGA functional with a semiempirical vdW correction[44,91] as implemented in QUANTUM ESPRESSO. HSE06 is known for its excellent treatment of the electronic structure of solids,[45,64] offering an excellent benchmark for PBE. For a test case, we chose polyyne at 5 molecules/nm^2 packing, aligned perpendicular to the surface—a high-dielectric constant monolayer. In comparison to the PBE results ($\varepsilon_{static} = 7.96$), we find $\varepsilon_{static} = 6.76$ for HSE06 and $\varepsilon_{static} = 7.91$ for vdW corrections. The screened hybrid functional is likely the most accurate value since HSE06 has demonstrated good accuracy in polarizability calculations on conjugated organics. While the HSE06 computed ε_{static} is somewhat lower, it is within 15% of the PBE result. Considering that the high computational demands of HSE06 prohibit extensive screening of the type reported here, and that elucidating trends are also of great importance, we believe that that the PBE functional is adequate for modeling the present study.

DISCUSSION

The results presented above reveal a number of intriguing strategies for modulating the molecular thin-film dielectric response. This discussion focuses on aiding the design of new high-capacitance organic gate dielectrics. The present results show that it is critically important in any high-dielectric molecular system to maximize the molecular packing density. For SAMs, this means achieving the highest 2-D packing density. A recent experimental study of SAM dielectric materials shows that a ~30% increase in surface coverage corresponds to ~30% increased capacitance.[33,34,46,47] Intuitively, this is reasonable since higher π-electron surface coverage fills a vacuum having a dielectric constant of 1. Nevertheless, maximizing surface coverage can be challenging for kinetic, electronic, and steric reasons. Additionally, controlling the orientation of dielectric molecular components is also important since many high-dielectric constant molecules have large anisotropies in their response. A disordered organic system is unlikely to achieve optimum dielectric response which may be one reason why champion organic dielectric materials are generally composed of molecular SAMs or other organized structures.[33,36,57,70,92] Fortuitously, repulsive dipole−dipole interactions have been shown to diminish with increasing surface coverage, due to generation of electric fields of opposite signs reducing dipole interactions within the plane, and making it easier to construct dense monolayer films.[48,83]

If materials properties are optimized, then obtaining high-capacitance organic dielectric constants becomes a molecular design question to maximize the electronic response of constituent molecules in bulk materials. The present work shows that different backbones and simple backbone substitutions can dramatically alter bulk dielectric performance in molecule-based dielectrics. In conjugated molecules, it is important that the molecule retain planarity to ensure maximum polarization of the π-system. Thus, interrupting planarity in donor−bridge−acceptor systems restricts donor−acceptor interactions and reduces the dielectric

response. In many cases, simple introduction of a polarizable substituent leads to significant response enhancements in systems that are already highly conjugated.

Functioning molecule-based TFT gate dielectric materials are typically composed of multiple structural components. For self-assembled nanodielectric materials, an oxide layer is deposited followed by an organic π-layer and finally capped with another inorganic layer to minimize leakage, ensure smooth deposition of the overlying TFT semiconductor, minimize $I-V_{gate}$ hysteresis, and preserve/enhance capacitance.[16,49] The parallel plate capacitor model is then used to compute the dielectric constant of a multilayer system (eq 4),[50,93] where d_i and ε_i are the thickness and dielectric constant, respectively, of component material i, d is the total thickness of the multilayer, and ε is the dielectric constant of the total multilayer. Equation 4 provides key insight into the dielectric response of a multilayer in that the dielectric constant of such structures is dominated by the behavior of the lowest dielectric constant material.

$$\frac{d}{\varepsilon} = \sum_{x}^{i=1} \frac{d_i}{\varepsilon_i} \qquad (4)$$

For example, in the bilayer system of Figure 9A, if a structure consisting of two dielectric component layers is considered where $d_1 = 5.0$ nm and $\varepsilon_1 = 20.0$, and $d_2 = 5.0$ nm with $\varepsilon_2 = 2.0$ and, the dielectric constant of the bilayer is found to be $\varepsilon = 3.64$, significantly closer to 2.0 than to 20.0. In fact, if ε_1 is doubled to 40.0, ε only increases to 3.80. In Figure 9B, the overall dielectric constant of a bilayer consisting of two different dielectric layers with equivalent thicknesses is shown. The dielectric constant of the entire stack cannot reach large values near $\varepsilon \sim 20.0$ unless both layers have a dielectric constant >15.0. In Figure 9C, the overall dielectric constant of a bilayer consisting of a 5 nm layer of SiO_2 with $\varepsilon = 3.90$ and a layer of variable thickness and dielectric constant is shown. Note that a 40 nm thick layer with $\varepsilon = 40.0$ is insufficient to raise the overall dielectric constant above 20.0 as long as the second layer is 5 nm SiO_2. Thus, introducing a low ε layer, even if it is far thinner than the accompanying layers, significantly diminishes the overall dielectric response. This necessitates that all components within a dielectric stack must have comparable dielectric constants. For developing multilayer hybrid molecule–oxide dielectrics, all constituent layers must share similar dielectric responses to achieve appreciable increases in the dielectric constant.

When designing FET gate dielectric materials, it is important to minimize leakage currents while maintaining large capacitance. In discussing conjugated *versus* nonconjugated SAM molecules above, the qualitative notion that molecules with extended

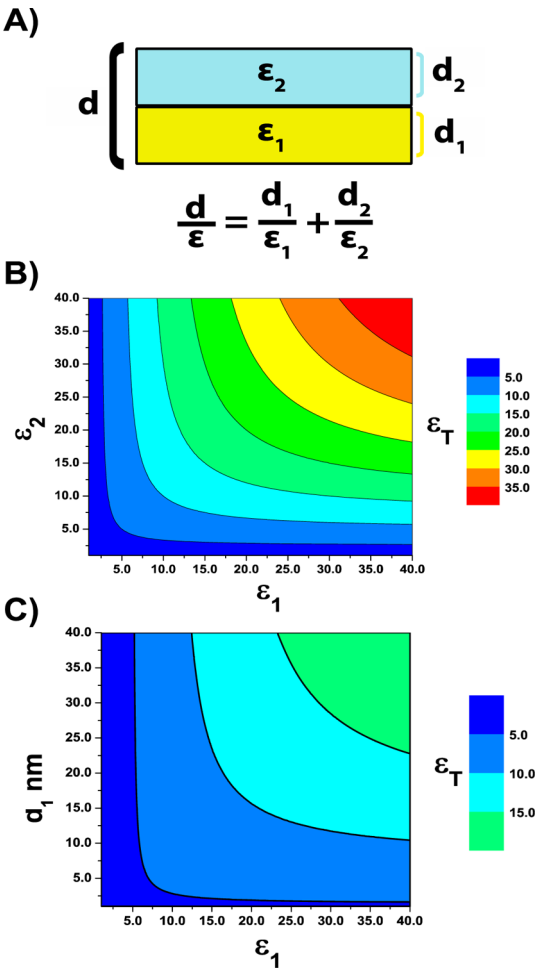

Figure 9. Total dielectric constants of bilayer dielectric systems. (A) Schematic of a two-slab system with each slab possessing a different dielectric constant. d_1 and d_2 represent thicknesses of slabs 1 and 2, respectively, while ε_1 and ε_2 represent the dielectric constant of each slab, and ε is the dielectric constant of the entire system with thickness d. (B) Overall dielectric constant as a function of ε_1 and ε_2. Each slab is assumed to have a thickness of 5 nm. (C) Overall dielectric constant of as a function of dielectric constant and thickness of slab 1. Slab 2 is assumed to be a 5 nm layer of SiO_2 with $\varepsilon_2 = 3.9$.

π-systems have larger dielectric responses than their saturated counterparts is quantified. It is of course well-known that highly polarizable molecules tend to have smaller band gaps,[51,94] and that classical inorganic materials have a well-established relationship between decreasing band gap and increasing dielectric constant.[52,95] A variety of band gap–refractive index empirical relationships also exist and are strongly dependent on the type of material.[36,57,96] Note that delocalized organic π-system materials can also transport charge,[97–100] potentially increasing leakage currents between the source/drain electrodes and the gate. Thus, the trade-off between dielectric constant and charge transport capability must be considered in designing high-capacitance organic dielectrics for FET applications and will be the subject of future studies.

CONCLUSIONS

Using a first-principles approach, the dielectric response of a number of linear and cyclic hydrocarbon molecule-based monolayer systems has been analyzed. From these calculations, much is learned about what molecular and materials properties afford large dielectric responses in such materials. In summary:

- In both the conjugated and nonconjugated systems, the optical and static dielectric constants are nearly identical. The dielectric response derives almost completely from the response of the electrons to the electric field.
- There is a linear relationship between thin-film molecular surface coverage and the dielectric constant of the resulting monolayer. Future development of large capacitance dielectric materials should focus on molecular systems that can achieve large packing densities.
- In conjugated systems, molecular orientation with respect to the electric field is critical for maximizing the dielectric constant, with the largest response occurring for π-systems aligned parallel to the applied field.
- Molecular geometry directly affects the dielectric response. Tuning molecular architecture in a given molecular materials system offers a means to tune the dielectric response.
- Different forms of conjugation along molecular backbones can afford moderate changes in the dielectric response. Introducing substituents having more polarizable atoms can significantly enhance the dielectric response.
- In large π-systems, addition of polarizable substituents can have only minor effects on the dielectric response.

These results offer important design rules for inventing new high-capacitance thin-film molecular dielectrics. In the present study, analysis primarily focused on hydrocarbon systems modeled as monolayers. A variety of other parameters should be analyzed when designing high-capacitance organic dielectrics. We emphasize that molecular composition *and* molecular environment are critical in altering the dielectric response of a molecular material. By optimizing surface coverage, tilt angle, and intermolecular interactions, the dielectric response of a molecular material can be significantly enhanced. While organic materials classes such as highly conjugated chromophores are promising candidates for high-capacitance organic dielectrics, peak dielectric response can only be achieved in specific architectures. A molecule can have a large computed polarizability, but without understanding how it assembles in the solid state, it is difficult to predict bulk dielectric response. Additionally, the trade-off between dielectric response and parasitic charge leakage should be considered when designing materials for dielectrics in capacitors. Striking a balance between dielectric response and current leakage will be critical in designing new low-voltage, highly efficient organic gate dielectrics.

METHODS

In the local dielectric description, a planar averaged induced charge density, $\overline{\rho}_{\mathrm{ind}}(z)$, is defined as in eq 5, where z is the axis parallel to the applied electric field and S is the xy cross-sectional area of the unit cell.

$$\overline{\rho}_{\mathrm{ind}}(z) = \frac{1}{S}\iint_{S}\Delta\rho\,\mathrm{d}x\mathrm{d}y \tag{5}$$

Note that $\overline{\rho}_{\mathrm{ind}}(z)$ is the difference in charge density in the presence of two different applied electric fields, E_1 and E_2 (eq 6). Therefore, all quantities reported are a function of the *difference* in electric field strengths of two applied electric fields.

$$\Delta\rho = \rho_2(x,y,z;E_2) - \rho_1(x,y,z;E_1) \tag{6}$$

This induced charge density can then be related to induced polarization, $\bar{P}(z)$, and change in total electric field due to an applied external field, $\bar{E}(z)$, using the definition of induced polarization (eq 7). Polarization can then be directly related to the planar-averaged local dielectric constant, $\eta(z)$, as in eq 8 with ε_0 the vacuum permittivity ($1/4\pi$).

$$\frac{d}{dz}\bar{P}(z) = -\overline{\rho}_{\mathrm{ind}}(z) \tag{7}$$

Furthermore

$$\eta(z) = \frac{\varepsilon_0 E_{\mathrm{ext}}}{\varepsilon_0 E_{\mathrm{ext}} - \bar{P}(z)} \tag{8}$$

$E_{\mathrm{ext}} = E_1 - E_2$, in this study, with the two applied electric fields always, $E_1 = -E_2$. The planar-averaged local dielectric constant, which is called $\eta(z)$ here, provides two informative quantities in monolayer systems. First, once the local dielectric response along a particular direction (*i.e.*, at a specific z coordinate) is known, a direct comparison between specific structural features and the corresponding dielectric response can be made. Second, while $\eta(z)$ is a nonmeasurable quantity, by applying a parallel plate capacitor model,[93] the experimentally observable dielectric constant ε can be computed using eq 9. Here η_i is the calculated local dielectric constant at a given index i along the z coordinate, the a and b indices correspond to the origin and terminus of the molecule, respectively, and ε is the dielectric constant averaged over the length of the molecule.

$$\frac{a-b}{\varepsilon} = \sum_{b}^{i=a}\frac{1}{\eta_i} \tag{9}$$

The origin and terminus of the molecule are defined as the positions along the z axis of the lowermost and uppermost constituent atoms, respectively, as shown in Figure 1.

The observable dielectric constant of a monolayer can also be calculated using the induced polarization of the entire monolayer, as shown by Natan[45] *et al.* and others. The relationship between polarization, P, of the monolayer and the dielectric constant, ε, is as in eq 10

$$\varepsilon = \frac{\varepsilon_0 E_{\mathrm{ext}}}{\varepsilon_0 E_{\mathrm{ext}} - P} \tag{10}$$

where ε_0 and E_{ext} are the same terms as used above. The polarization for the monolayer is then defined as

$$P = \frac{\Delta\mu}{V_{ML}} \tag{11}$$

where $\Delta\mu$ is the change in dipole moment of the monolayer induced by an applied field and V_{ML} is the volume of the monolayer. V_{ML} is the area of the unit cell times the thickness of the monolayer ($a - b$ in Figure 1). The calculated ε is theoretically identical in eqs 9 and 10;[45] however, there are numerical discrepancies between the two values for highly polarizable molecules. This is caused by locally large polarization that causes eq 8 to diverge. If the local polarization is properly averaged,[53] then the two values agree. In this investigation, we utilize both methods to calculate the dielectric response. The local dielectric method is desirable when analyzing local dielectric effects in a material, while the dipole method is more robust for highly polarizable materials and is easier to execute. Any data referencing local dielectric behavior (η) were obtained using the local dielectric method (eq 9), while dielectric constants (ε) are found using the dipole method (eq 10).

The optical dielectric constant, ε_o, is the high-frequency $\omega \rightarrow \infty$ dielectric constant and is calculated assuming that only the electrons respond to the oscillating electric field (*i.e.*, optical regime). The static dielectric constant, ε_s, is the low-frequency $\omega \rightarrow 0$ dielectric constant and is calculated by allowing the internal molecular geometry to relax in the presence of the electric field. In both the optical and static responses, no molecular translational or rotational motion is allowed. The calculations were performed using DFT within the generalized gradient approximation (GGA) as implemented by the Perdew–Burke–Ernzerhof (PBE)[101] functional and Vanderbilt ultrasoft pseudopotentials,[102] as implemented in QUANTUM ESPRESSO.[103] Explicit surfaces are not modeled because numerous studies have shown that dielectric response is highly localized and that interface effects are minor beyond 2–3 Å.[33,45,53,104] Adding an explicit oxide surface would dramatically increase computation time with little added insight. GGA functionals have been used in a variety of dielectric calculations, including polar and nonpolar organic multilayers,[33] phthalocyanine ribbons,[89,105] metal oxides,[54,56] metal oxide/metal oxide interfaces,[90] and metal oxide/organic interfaces,[53] and have proven accurate, typically matching experimental dielectric constants within ~10%. It is known that GGA functionals typically overestimate polarizability in conjugated materials; therefore, our calculated results likely represent upper bounds for experimental dielectric constants but are still instructive and of useful accuracy (see more below).[106,107] In the Results section, we show the validity of this model by comparing computed results with experimental values from the literature and examine how functional choice effects computed values. For all calculations, forces were relaxed to 10 meV/Å. The wave functions and the augmented charge density are represented by plane-wave basis sets with energy cutoffs of 60 and 660 Ry, respectively. Unless otherwise stated, an applied field of 0.001 au is used. We previously found that using electric fields of this magnitude has no effect on the results.[33] Note that electric field strengths greater than 10^{-2} au often lead to SCF convergence difficulties; however, the field strength investigated here is within the range used in experiment.[24] Polarizabilities are calculated using finite differences with the ωB97X[108] functional and an aug-cc-PVDZ basis set within GAMESS[109] and closely match values reported on the NIST database.[110]

Conflict of Interest: The authors declare no competing financial interest.

Acknowledgment. The research was supported by the MRSEC program of NSF (DMR-1121262) through the Northwestern University Materials Research Center. H.M.H. is supported by the Department of Defense (DoD) through the National Defense Science & Engineering Graduate Fellowship (NDSEG) Program.

REFERENCES AND NOTES

1. Mas-Torrent, M.; Rovira, C. Novel Small Molecules for Organic Field-Effect Transistors: Towards Processability and High Performance. *Chem. Soc. Rev.* **2008**, *37*, 827–838.
2. Gelinck, G. H.; Huitema, H. E. A.; van Veenendaal, E.; Cantatore, E.; Schrijnemakers, L.; van der Putten, J. B. P. H.; Geuns, T. C. T.; Beenhakkers, M.; Giesbers, J. B.; Huisman, B.-H.; *et al.* Flexible Active-Matrix Displays and Shift Registers Based on Solution-Processed Organic Transistors. *Nat. Mater.* **2004**, *3*, 106–110.
3. Allard, S.; Forster, M.; Souharce, B.; Thiem, H.; Scherf, U. Organic Semiconductors for Solution-Processable Field-Effect Transistors (OFETs). *Angew. Chem., Int. Ed.* **2008**, *47*, 4070–4098.
4. Arias, A. C.; MacKenzie, J. D.; McCulloch, I.; Rivnay, J.; Salleo, A. Materials and Applications for Large Area Electronics: Solution-Based Approaches. *Chem. Rev.* **2010**, *110*, 3–24.
5. Wen, Y.; Liu, Y. Recent Progress in N-Channel Organic Thin-Film Transistors. *Adv. Mater.* **2010**, *22*, 1331–1345.
6. Dickey, K. C.; Subramanian, S.; Anthony, J. E.; Han, L.-H.; Chen, S.; Loo, Y.-L. Large-Area Patterning of a Solution-Processable Organic Semiconductor to Reduce Parasitic Leakage and Off Currents in Thin-Film Transistors. *Appl. Phys. Lett.* **2007**, *90*, 244103.
7. Usta, H.; Facchetti, A.; Marks, T. J. N-Channel Semiconductor Materials Design for Organic Complementary Circuits. *Acc. Chem. Res.* **2011**, *44*, 501–510.
8. Hagleitner, C.; Hierlemann, A.; Lange, D.; Kummer, A.; Kerness, N.; Brand, O.; Baltes, H. Smart Single-Chip Gas Sensor Microsystem. *Nature* **2001**, *414*, 293–296.
9. Sokolov, A. N.; Tee, B. C.-K.; Bettinger, C. J.; Tok, J. B.-H.; Bao, Z. Chemical and Engineering Approaches To Enable Organic Field-Effect Transistors for Electronic Skin Applications. *Acc. Chem. Res.* **2012**, *45*, 361–371.
10. Sherry, L. J.; Chang, S.-H.; Schatz, G. C.; Van Duyne, R. P.; Wiley, B. J.; Xia, Y. Localized Surface Plasmon Resonance Spectroscopy of Single Silver Nanocubes. *Nano Lett.* **2005**, *5*, 2034–2038.
11. Sirringhaus, H. Materials and Applications for Solution-Processed Organic Field-Effect Transistors. *Proc. IEEE* **2009**, *97*, 1570–1579.
12. Tobjörk, D.; Österbacka, R. Paper Electronics. *Adv. Mater.* **2011**, *23*, 1935–1961.
13. Kergoat, L.; Herlogsson, L.; Piro, B.; Pham, M. C.; Horowitz, G.; Crispin, X.; Berggren, M. Tuning the Threshold Voltage in Electrolyte-Gated Organic Field-Effect Transistors. *Proc. Natl. Acad. Sci. U.S.A.* **2012**, *109*, 8394–8399.
14. Horowitz, G. Organic Field-Effect Transistors. *Adv. Mater.* **1998**, *10*, 365–377.
15. DiBenedetto, S. A.; Facchetti, A.; Ratner, M. A.; Marks, T. J. Molecular Self-Assembled Monolayers and Multilayers for Organic and Unconventional Inorganic Thin-Film Transistor Applications. *Adv. Mater.* **2009**, *21*, 1407–1433.
16. Ortiz, R. P.; Facchetti, A.; Marks, T. J. High-K Organic, Inorganic, and Hybrid Dielectrics for Low-Voltage Organic Field-Effect Transistors. *Chem. Rev.* **2010**, *110*, 205–239.
17. Ha, Y.-G.; Everaerts, K.; Hersam, M. C.; Marks, T. J. Hybrid Gate Dielectric Materials for Unconventional Electronic Circuitry. *Acc. Chem. Res.* **2014**, *47*, 1019–1028.
18. Horowitz, G. Cambridge Journals Online - Abstract - Organic Thin Film Transistors: From Theory to Real Devices. *J. Mater. Res.* **2004**, *19*, 1946–1962.
19. Tsumura, A.; Koezuka, H.; Ando, T. Macromolecular Electronic Device: Field-Effect Transistor with a Polythiophene Thin Film. *Appl. Phys. Lett.* **1986**, *49*, 1210–1212.
20. Sorsch, T.; Timp, W.; Baumann, F. H.; Bogart, K. H. A.; Boone, T.; Donnelly, V. M.; Green, M.; Evans-Lutterodt, K.; Kim, C. Y.; Moccio, S.; *et al.* Ultra-Thin, 1.0–3.0nm, Gate Oxides for High Performance Sub-100 nm Technology. *Symp. VLSI Technol., Dig. Tech. Pap.* **1998**, *22*, 222–223.
21. Momose, H. S.; Ono, M.; Yoshitomi, T.; Ohguro, T.; Nakamura, S.; Saito, M.; Iwai, H. Tunneling Gate Oxide

Approach to Ultra-High Current Drive in Small-Geometry MOSFETs. *Tech. Dig. - IEEE* **1994**, 593–596.
22. Nagano, S.; Tsukiji, M.; Ando, K.; Hasegawa, E.; Ishitani, A. Mechanism of Leakage Current through the Nanoscale SiO_2 Layer. *J. Appl. Phys.* **1994**, *75*, 3530–3535.
23. Henisch, H. K.; Manifacier, J. C. Space-Charge Conduction and Relaxation in Dielectric Films. *J. Appl. Phys.* **1987**, *61*, 5379–5385.
24. DiBenedetto, S. A.; Facchetti, A.; Ratner, M. A.; Marks, T. J. Charge Conduction and Breakdown Mechanisms in Self-Assembled Nanodielectrics. *J. Am. Chem. Soc.* **2009**, *131*, 7158–7168.
25. Eisenberg, H. R.; Baer, R. A New Generalized Kohn-Sham Method for Fundamental Band-Gaps in Solids. *Phys. Chem. Chem. Phys.* **2009**, *11*, 4674–4680.
26. Rampi, M.; Schueller, O.; Whitesides, G. Alkanethiol Self-Assembled Monolayers as the Dielectric of Capacitors with Nanoscale Thickness. *Appl. Phys. Lett.* **1998**, *72*, 1781–1783.
27. Slowinski, K.; Chamberlain, R. V.; Miller, C. J.; Majda, M. Through-Bond and Chain-to-Chain Coupling. Two Pathways in Electron Tunneling through Liquid Alkanethiol Monolayers on Mercury Electrodes. *J. Am. Chem. Soc.* **1997**, *119*, 11910–11919.
28. Braga, D.; Horowitz, G. High-Performance Organic Field-Effect Transistors. *Adv. Mater.* **2009**, *21*, 1473–1486.
29. Sirringhaus, H.; Sakanoue, T. Charge-Transport Physics of High-Mobility Molecular Semiconductors. *Phys. Status Solidi B* **2012**, *249*, 1655–1676.
30. Anthony, J. E.; Facchetti, A.; Heeney, M.; Marder, S. R.; Zhan, X. n-Type Organic Semiconductors in Organic Electronics. *Adv. Mater.* **2010**, *22*, 3876–3892.
31. Klauk, H.; Zschieschang, U.; Pflaum, J.; Halik, M. Ultralow-Power Organic Complementary Circuits. *Nature* **2007**, *445*, 745–748.
32. Dressel, M.; Gompf, B.; Faltermeier, D.; Tripathi, A. K.; Pflaum, J.; Schubert, M. Kramers-Kronig-Consistent Optical Functions of Anisotropic Crystals: Generalized Spectroscopic Ellipsometry on Pentacene. *Opt. Express* **2008**, *16*, 19770–19778.
33. Heitzer, H. M.; Marks, T. J.; Ratner, M. A. First-Principles Calculation of Dielectric Response in Molecule-Based Materials. *J. Am. Chem. Soc.* **2013**, *135*, 9753–9759.
34. Everaerts, K.; Emery, J. D.; Jariwala, D.; Karmel, H. J.; Sangwan, V. K.; Prabhumirashi, P. L.; Geier, M. L.; McMorrow, J. J.; Bedzyk, M. J.; Facchetti, A.; *et al.* Ambient-Processable High Capacitance Hafnia-Organic Self-Assembled Nanodielectrics. *J. Am. Chem. Soc.* **2013**, *135*, 8926–8939.
35. Yoon, M.-H.; Kim, C.; Facchetti, A.; Marks, T. J. Gate Dielectric Chemical Structure-Organic Field-Effect Transistor Performance Correlations for Electron, Hole, and Ambipolar Organic Semiconductors. *J. Am. Chem. Soc.* **2006**, *128*, 12851–12869.
36. Ting, G. G., II; Acton, O.; Ma, H.; Ka, J. W.; Jen, A. K. Y. Study on the Formation of Self-Assembled Monolayers on Sol–Gel Processed Hafnium Oxide as Dielectric Layers. *Langmuir* **2009**, *25*, 2140–2147.
37. Sharma, V.; Wang, C.; Lorenzini, R. G.; Ma, R.; Zhu, Q.; Sinkovits, D. W.; Pilania, G.; Oganov, A. R.; Kumar, S.; Sotzing, G. A.; *et al.* Rational Design of All Organic Polymer Dielectrics. *Nat. Commun.* **2014**, *5*, 4845.
38. Brédas, J.-L.; Norton, J. E.; Cornil, J.; Coropceanu, V. Molecular Understanding of Organic Solar Cells: The Challenges. *Acc. Chem. Res.* **2009**, *42*, 1691–1699.
39. Veinot, J.; Marks, T. J. Toward the Ideal Organic Light-Emitting Diode. The Versatility and Utility of Interfacial Tailoring by Cross-Linked Siloxane Interlayers. *Acc. Chem. Res.* **2005**, *38*, 632–643.
40. Marcus, R. A. Electron Transfer Reactions in Chemistry Theory and Experiment. *J. Electroanal. Chem.* **1997**, *438*, 251–259.
41. Maroncelli, M.; Macinnis, J.; Fleming, G. R. Polar Solvent Dynamics and Electron-Transfer Reactions. *Science* **1989**, *243*, 1674–1681.
42. Mannsfeld, S. C. B.; Tee, B. C.-K.; Stoltenberg, R. M.; Chen, C. V. H.-H.; Barman, S.; Muir, B. V. O.; Sokolov, A. N.; Reese, C.; Bao, Z. Highly Sensitive Flexible Pressure Sensors with Microstructured Rubber Dielectric Layers. *Nat. Mater.* **2010**, *9*, 859–864.
43. Blythe, A. R.; Bloor, D. *Electrical Properties of Polymers*, 2nd ed.; Cambridge University Press: Cambridge, U.K., 2005.
44. DiBenedetto, S. A.; Frattarelli, D. L.; Facchetti, A.; Ratner, M. A.; Marks, T. J. Structure-Performance Correlations in Vapor Phase Deposited Self-Assembled Nanodielectrics for Organic Field-Effect Transistors. *J. Am. Chem. Soc.* **2009**, *131*, 11080–11090.
45. Natan, A.; Kuritz, N.; Kronik, L. Polarizability, Susceptibility, and Dielectric Constant of Nanometer-Scale Molecular Films: A Microscopic View. *Adv. Funct. Mater.* **2010**, *20*, 2077–2084.
46. Day, B. S.; Morris, J. R. Packing Density and Structure Effects on Energy-Transfer Dynamics in Argon Collisions with Organic Monolayers. *J. Chem. Phys.* **2005**, *122*, 234714.
47. George, C.; Yoshida, H.; Goddard, W. A.; Jang, S. S.; Kim, Y.-H. Charge Transport through Polyene Self-Assembled Monolayers From Multiscale Computer Simulations. *J. Phys. Chem. B* **2008**, *112*, 14888–14897.
48. Takacs, C. J.; Sun, Y.; Welch, G. C.; Perez, L. A.; Liu, X.; Wen, W.; Bazan, G. C.; Heeger, A. J. Solar Cell Efficiency, Self-Assembly, and Dipole–Dipole Interactions of Isomorphic Narrow-Band-Gap Molecules. *J. Am. Chem. Soc.* **2012**, *134*, 16597–16606.
49. Bredas, J. L. Relationship between Band Gap and Bond Length Alternation in Organic Conjugated Polymers. *J. Chem. Phys.* **1985**, *82*, 3808–3811.
50. Ma, W.; Tumbleston, J. R.; Wang, M.; Gann, E.; Huang, F.; Ade, H. Domain Purity, Miscibility, and Molecular Orientation at Donor/Acceptor Interfaces in High Performance Organic Solar Cells: Paths to Further Improvement. *Adv. Energy Mater.* **2013**, *3*, 864–872.
51. Yang, C.; Yoon, J.; Kim, S. H.; Hong, K.; Chung, D. S.; Heo, K.; Park, C. E.; Ree, M. Bending-Stress-Driven Phase Transitions in Pentacene Thin Films for Flexible Organic Field-Effect Transistors. *Appl. Phys. Lett.* **2008**, *92*, 243305.
52. Sokolov, A. N.; Cao, Y.; Johnson, O. B.; Bao, Z. Mechanistic Considerations of Bending-Strain Effects within Organic Semiconductors on Polymer Dielectrics. *Adv. Funct. Mater.* **2011**, *22*, 175–183.
53. Yu, L.; Ranjan, V.; Nardelli, M.; Bernholc, J. First-Principles Investigations of the Dielectric Properties of Polypropylene/Metal-Oxide Interfaces. *Phys. Rev. B* **2009**, *80*, 165432.
54. Pilania, G.; Ramprasad, R. Dielectric Permittivity of Ultrathin $PbTiO_3$ Nanowires From First Principles. *J. Mater. Sci.* **2012**, *47*, 7580–7586.
55. Rignanese, G.-M.; Detraux, F.; Gonze, X.; Bongiorno, A.; Pasquarello, A. Dielectric Constants of Zr Silicates: A First-Principles Study. *Phys. Rev. Lett.* **2002**, *89*, 117601.
56. Ramprasad, R.; Shi, N. Dielectric Properties of Nanoscale HfO_2 Slabs. *Phys. Rev. B* **2005**, *72*, 052107–052101.
57. Yoon, M. H. Molecular Dielectric Multilayers for Low-Voltage Organic Thin-Film Transistors. *Proc. Natl. Acad. Sci. U.S.A.* **2005**, *102*, 4678–4682.
58. Deibel, C.; Dyakonov, V. Polymer–Fullerene Bulk Heterojunction Solar Cells. *Rep. Prog. Phys.* **2010**, *73*, 096401.
59. Mishra, A.; Ma, C.-Q.; Bäuerle, P. Functional Oligothiophenes: Molecular Design for Multidimensional Nanoarchitectures and Their Applications. *Chem. Rev.* **2009**, *109*, 1141–1276.
60. Ulman, A. Formation and Structure of Self-Assembled Monolayers. *Chem. Rev.* **1996**, *96*, 1534–1554.
61. Love, J. C.; Estroff, L. A.; Kriebel, J. K.; Nuzzo, R. G.; Whitesides, G. M. Self-Assembled Monolayers of Thiolates on Metals as a Form of Nanotechnology. *Chem. Rev.* **2005**, *105*, 1103–1169.
62. van Gisbergen, S.; Schipper, P.; Gritsenko, O.; Baerends, E.; Snijders, J.; Champagne, B.; Kirtman, B. Electric Field Dependence of the Exchange-Correlation Potential in Molecular Chains. *Phys. Rev. Lett.* **1999**, *83*, 694–697.

63. Janesko, B. G. Comparing Modern Density Functionals for Conjugated Polymer Band Structures: Screened Hybrid, Minnesota, and Rung 3.5 Approximations. *J. Chem. Phys.* **2011**, *134*, 184105.
64. Henderson, T. M.; Paier, J.; Scuseria, G. E. Accurate Treatment of Solids with the HSE Screened Hybrid. *Phys. Status Solidi B* **2010**, *248*, 767–774.
65. Sekino, H.; Maeda, Y.; Kamiya, M.; Hirao, K. Polarizability and Second Hyperpolarizability Evaluation of Long Molecules by the Density Functional Theory with Long-Range Correction. *J. Chem. Phys.* **2007**, *126*, 014107.
66. Kudin, K. N.; Car, R.; Resta, R. Longitudinal Polarizability of Long Polymeric Chains: Quasi-One-Dimensional Electrostatics as the Origin of Slow Convergence. *J. Chem. Phys.* **2005**, *122*, 134907.
67. Romaner, L.; Heimel, G.; Ambrosch-Draxl, C.; Zojer, E. The Dielectric Constant of Self-Assembled Monolayers. *Adv. Funct. Mater.* **2008**, *18*, 3999–4006.
68. Natan, A.; Zidon, Y.; Shapira, Y.; Kronik, L. Cooperative Effects and Dipole Formation at Semiconductor and Self-Assembled-Monolayer Interfaces. *Phys. Rev. B* **2006**, *73*, 193310.
69. Peor, N.; Sfez, R.; Yitzchaik, S. Variable Density Effect of Self-Assembled Polarizable Monolayers on the Electronic Properties of Silicon. *J. Am. Chem. Soc.* **2008**, *130*, 4158–4165.
70. Halik, M.; Klauk, H.; Zschieschang, U.; Schmid, G.; Dehm, C.; Schütz, M.; Maisch, S.; Effenberger, F.; Brunnbauer, M.; Stellacci, F. Low-Voltage Organic Transistors with an Amorphous Molecular Gate Dielectric. *Nature* **2004**, *431*, 963–966.
71. Pal, B. N.; Dhar, B. M.; See, K. C.; Katz, H. E. Solution-Deposited Sodium Beta-Alumina Gate Dielectrics for Low-Voltage and Transparent Field-Effect Transistors. *Nat. Mater.* **2010**, *9*, 279–279.
72. Amin, B.; Nazir, S.; Schwingenschlögl, U. Molecular Distortion and Charge Transfer Effects in ZnPc/Cu(111). *Sci. Rep.* **2013**, *3*, 1705.
73. Otto, R.; Brox, J.; Trippel, S.; Stei, M.; Best, T.; Wester, R. Single Solvent Molecules Can Affect the Dynamics of Substitution Reactions. *Nat. Chem.* **2012**, *4*, 534–538.
74. Li, C.; Tan, T.; Zhang, H.; Feng, W. Analysis of the Conformational Stability and Activity of *Candida antarctica* Lipase B in Organic Solvents: Insight from Molecular Dynamics and Quantum Mechanics/Simulations. *J. Biol. Chem.* **2010**, *285*, 28434–28441.
75. Grein, F. Twist Angles and Rotational Energy Barriers of Biphenyl and Substituted Biphenyls. *J. Phys. Chem. A* **2002**, *106*, 3823–3827.
76. Johansson, M. P.; Olsen, J. Torsional Barriers and Equilibrium Angle of Biphenyl: Reconciling Theory with Experiment. *J. Chem. Theory Comput.* **2008**, *4*, 1460–1471.
77. Albinsson, B.; Eng, M. P.; Pettersson, K.; Winters, M. U. Electron and Energy Transfer in Donor–Acceptor Systems with Conjugated Molecular Bridges. *Phys. Chem. Chem. Phys.* **2007**, *9*, 5847–5864.
78. Terao, J.; Wadahama, A.; Matono, A.; Tada, T.; Watanabe, S.; Seki, S.; Fujihara, T.; Tsuji, Y. Design Principle for Increasing Charge Mobility of π-Conjugated Polymers Using Regularly Localized Molecular Orbitals. *Nat. Commun.* **2013**, *4*, 1691.
79. Ahmed, A.; Bragg, R. A.; Clayden, J.; Lai, L. W.; McCarthy, C.; Pink, J. H.; Westlund, N.; Yasin, S. A. Barriers to Rotation About the Chiral Axis of Tertiary Aromatic Amides. *Tetrahedron* **1998**, *54*, 13277–13294.
80. Ramprasad, R.; Shi, N. Polarizability of Phthalocyanine Based Molecular Systems: A First-Principles Electronic Structure Study. *Appl. Phys. Lett.* **2006**, *88*, 222903.
81. Wang, Y.; Kröger, J.; Berndt, R.; Hofer, W. A. Pushing and Pulling a Sn Ion through an Adsorbed Phthalocyanine Molecule. *J. Am. Chem. Soc.* **2009**, *131*, 3639–3643.
82. Strohmaier, R.; Ludwig, C.; Petersen, J. Scanning Tunneling Microscope Investigations of Lead–Phthalocyanine on MoS_2. *J. Vac. Sci. Technol., B* **1996**, *14*, 1079–1082.
83. Deshlahra, P.; Conway, J.; Wolf, E. E.; Schneider, W. F. Influence of Dipole–Dipole Interactions on Coverage-Dependent Adsorption: CO and NO on Pt(111). *Langmuir* **2012**, *28*, 8408–8417.
84. Porter, M. D.; Bright, T. B.; Allara, D. L.; Chidsey, C. E. D. Spontaneously Organized Molecular Assemblies. 4. Structural Characterization of *N*-Alkyl Thiol Monolayers on Gold by Optical Ellipsometry, Infrared Spectroscopy, and Electrochemistry. *J. Am. Chem. Soc.* **1987**, *109*, 3559–3568.
85. Miller, C.; Cuendet, P.; Graetzel, M. Adsorbed ω-Hydroxy Thiol Monolayers on Gold Electrodes: Evidence for Electron Tunneling to Redox Species in Solution. *J. Phys. Chem.* **1991**, *95*, 877–886.
86. Akkerman, H. B.; Naber, R. C. G.; Jongbloed, B.; van Hal, P. A.; Blom, P. W. M.; de Leeuw, D. M.; de Boer, B. Electron Tunneling through Alkanedithiol Self-Assembled Monolayers in Large-Area Molecular Junctions. *Proc. Natl. Acad. Sci. U.S.A.* **2007**, *104*, 11161–11166.
87. Chidsey, C. E. D. Free Energy and Temperature Dependence of Electron Transfer at the Metal–Electrolyte Interface. *Science* **1991**, *251*, 919–922.
88. Everaerts, K.; Emery, J. D.; Jariwala, D.; Karmel, H. J.; Sangwan, V. K.; Prabhumirashi, P. L.; Geier, M. L.; McMorrow, J. J.; Bedzyk, M. J.; Facchetti, A.; *et al.* Ambient-Processable High Capacitance Hafnia-Organic Self-Assembled Nanodielectrics. *J. Am. Chem. Soc.* **2013**, *135*, 8926–8939.
89. Shi, N.; Ramprasad, R. Dielectric Properties of Cu-Phthalocyanine Systems from First Principles. *Appl. Phys. Lett.* **2006**, *89*, 102904.
90. Giustino, F.; Pasquarello, A. Theory of Atomic-Scale Dielectric Permittivity at Insulator Interfaces. *Phys. Rev. B* **2005**, *71*, 144104.
91. Grimme, S. Semiempirical GGA-Type Density Functional Constructed with a Long-Range Dispersion Correction. *J. Comput. Chem.* **2006**, *27*, 1787–1799.
92. Everaerts, K.; Emery, J. D.; Jariwala, D.; Karmel, H. J.; Sangwan, V. K.; Prabhumirashi, P. L.; Geier, M. L.; McMorrow, J. J.; Bedzyk, M. J.; Facchetti, A.; *et al.* Ambient-Processable High Capacitance Hafnia-Organic Self-Assembled Nanodielectrics. *J. Am. Chem. Soc.* **2013**, *135*, 8926–8939.
93. Sze, S. M.; Lee, M.-K. *Semiconductor Devices: Physics and Technology*, 3rd ed.; Wiley: New York, 2012.
94. Alyar, H. A Review on Nonlinear Optical Properties of Donor–Acceptor Derivatives of Naphthalene and Azanaphthalene. *Rev. Adv. Mater. Sci.* **2013**, *34*, 79–87.
95. Robertson, J. High Dielectric Constant Oxides. *Eur. Phys. J. Appl. Phys.* **2004**, *28*, 265–291.
96. Ravindra, N. M.; Ganapathy, P.; Choi, J. Energy Gap–Refractive Index Relations in Semiconductors—An Overview. *Infrared Phys. Technol.* **2007**, *50*, 21–29.
97. Shirakawa, H. The Discovery of Polyacetylene Film: The Dawning of an Era of Conducting Polymers. *Angew. Chem., Int. Ed.* **2001**, *40*, 2574–2580.
98. Nitzan, A.; Ratner, M. A. Electron Transport in Molecular Wire Junctions. *Science* **2003**, *300*, 1384–1389.
99. Facchetti, A. π-Conjugated Polymers for Organic Electronics and Photovoltaic Cell Applications. *Chem. Mater.* **2011**, *23*, 733–758.
100. Usta, H.; Risko, C.; Wang, Z.; Huang, H.; Deliomeroglu, M. K.; Zhukhovitskiy, A.; Facchetti, A.; Marks, T. J. Design, Synthesis, and Characterization of Ladder-Type Molecules and Polymers. Air-Stable, Solution-Processable N-Channel and Ambipolar Semiconductors for Thin-Film Transistors *via* Experiment and Theory. *J. Am. Chem. Soc.* **2009**, *131*, 5586–5608.
101. Perdew, J.; Burke, K.; Ernzerhof, M. Generalized Gradient Approximation Made Simple. *Phys. Rev. Lett.* **1996**, *77*, 3865–3868.
102. Vanderbilt, D. Soft Self-Consistent Pseudopotentials in a Generalized Eigenvalue Formalism. *Phys. Rev. B* **1990**, *41*, 7892–7895.

103. Giannozzi, P.; Baroni, S.; Bonini, N.; Calandra, M.; Car, R.; Cavazzoni, C.; Ceresoli, D.; Chiarotti, G. L.; Cococcioni, M.; Dabo, I.; *et al.* QUANTUM ESPRESSO: A Modular and Open-Source Software Project for Quantum Simulations of Materials. *J. Phys.: Condens. Matter* **2009**, *21*, 395502.
104. Shi, N.; Ramprasad, R. Atomic-Scale Dielectric Permittivity Profiles in Slabs and Multilayers. *Phys. Rev. B* **2006**, *74*, 045318.
105. Shi, N.; Ramprasad, R. Intrinsic Dielectric Properties of Phthalocyanine Crystals: An *Ab Initio* Investigation. *Phys. Rev. B* **2007**, *75*, 155429.
106. Champagne, B.; Perpète, E. A.; van Gisbergen, S. J. A.; Baerends, E.-J.; Snijders, J. G.; Soubra-Ghaoui, C.; Robins, K. A.; Kirtman, B. Assessment of Conventional Density Functional Schemes for Computing the Polarizabilities and Hyperpolarizabilities of Conjugated Oligomers: An *Ab Initio* Investigation of Polyacetylene Chains. *J. Chem. Phys.* **1998**, *109*, 10489–10498.
107. McDowell, S. A. C.; Amos, R. D.; Handy, N. C. Molecular Polarisabilities—A Comparison of Density Functional Theory with Standard *Ab Initio* Methods. *Chem. Phys. Lett.* **1995**, *235*, 1–4.
108. Chai, J.-D.; Head-Gordon, M. Systematic Optimization of Long-Range Corrected Hybrid Density Functionals. *J. Chem. Phys.* **2008**, *128*, 084106.
109. Schmidt, M. W.; Baldridge, K. K.; Boatz, J. A. General Atomic and Molecular Electronic Structure System. *J. Comput. Chem.* **1993**, *14*, 1347–1363.
110. *NIST Computational Chemistry Comparison and Benchmark Database*; Johnson, R. D., III, Ed.; 16th ed.; NIST Standard Reference Database Number 101, 2013.